Robust Hierarchical Density Estimation and Regression for Re-stained Histological Whole Slide Image Co-registration

Jun Jiang[1#a], Nicholas B. Larson[1#b], Naresh Prodduturi[1#c], Thomas J. Flotte[#d], Steven N. Hart[1#e*]

[1#]Deparment of Health Science Research Mayo Clinic, Rochester, Minnesota, United States of America

[2]Department of Anatomic Pathology, Mayo Clinic, Rochester, Minnesota, United States of America

[#a]Mayo Clinic, Harwick 3, 200 First Street SW, Rochester, Minnesota, United States of America

[#b]Mayo Clinic, Harwick 7-32, 200 First Street SW, Rochester, Minnesota, United States of America

[#c]Mayo Clinic, Harwick 3-02-38, 200 First Street SW, Rochester, Minnesota, United States of America

[#d]Mayo Clinic, Hilton Building 11, 200 First Street SW, Rochester, Minnesota, United States of America

[#e]Mayo Clinic, Harwick 3-13, 200 First Street SW, Rochester, Minnesota, United States of America

*Corresponding Author
Hart.Steven@mayo.edu

Short Title: Image Co-Registration with KDE

Keywords: Digital Pathology, Image Registration, Whole Slide Images, Bioinformatics, Image Processing

Authors Contributions: Study design – SNH; Subject matter expertise – TJF; Approach development – SNH, JJ, NL, NP. All authors read and approved manuscript.

Disclosure of Potential Conflicts of Interest: No potential conflicts of interest were disclosed

Abstract

For many conditions, tissue samples are colored with multiple dyes and stains to add contrast, identify specific and general classes of chemicals in order to accurately identify and diagnose disease. This presents a computational challenge for digital pathology, as entire whole-slide images (WSIs) need to be overlaid to identify co-localized features. Traditional image registration methods sometimes fail due to the high variation of cell density and insufficient texture information in WSIs – particularly at high magnifications. In this paper, we proposed a robust image co-registration strategy to align stained, destained, and re-stained WSIs precisely and efficiently. This method is applied to three immunohistochemical (IHC) stains with their hematoxylin and eosin (H&E) counterparts. Our approach advances the existing methods in three key aspects. First, we present a framework that incorporates fundamental image registration with refinement methods. Second, we present an effective weighting strategy using kernel density estimation to mitigate registration errors. Third, we account for the linear relationship across WSI levels to improve accuracy. Our experiments show higher accuracy on matching IHC and H&E pairs, enabling subcellular-level analysis on stained and re-stained histological images. We also provide a tool to allow users to develop their own registration benchmarking experiments.

Introduction

Histological assessment is a critically important feature in the diagnosis, prognosis, and treatment of disease. Until recently, tissues were only viewed under a traditional light microscope. Two of the most prominent examples of tissue staining are hematoxylin & eosin (H&E) and immunohistochemistry (IHC). However, with the advancement of digital pathology, high-throughput whole-slide scanners are increasingly being used – enabling a more quantitative assessment of histologic features on whole-slide images (WSIs). There are multiple scenarios for studying co-localized stains. In the first case, two serial sections can be taken from a tissue and stained with different chemicals. Alternatively, a slide could be stained with one reagent, imaged, destained, re-stained with another reagent and imaged again. Biological tissues can vary architecturally and in composition at the submicron level. For this reason, adjacent sections can be sampling dramatically different chemical compositions. The stain-restain method provides more accurate correlation of the chemicals of interest. A third approach is multiplexed imaging, however, not all stains can be imaged with this approach.

From a computational perspective, this means the stain-restain scenario is more suitable for rigid image registration, while the former is more suitable for non-rigid image registration. Most of the previous work in the WSI registration field has been focused on aligning consecutive sections of tissues for cross-sectional observations (e.g., 3-dimensional tissue visualization) [1-5]. Moreover, methods such as those proposed by Mueller et al. [6] use a deformable multi-modal WSI registration technique. Using deformable registration does not explicitly model the fact that pixels in multi-modal images may not belong to the same cell, which can introduce errors into downstream analysis. In this paper, we focused on re-stained histological WSI co-registration, which uses a rigid image registration strategy that allows co-locating multiple markers in the same cell for more complex quantitative analysis.

The need for a rigid image registration is based on the fact that re-stained tissues have a fixed relative position to the slide glass, meaning there should be some (x, y) shifting, but no rotation. Several state-of-the-art rigid image registration methods could potentially be used to handle this problem. Scale-Invariant Feature Transform (SIFT) [7] is one of the most popular “key points”-based image registration method, in which strongly differentiable pixel areas are detected, filtered, and matched based on their local features. Key points can be filtered based on the differences in slope between matched key point pairs. In other words, lines connecting matched pairs of key points in the stationary and corresponding floating image should be parallel. Enhanced Correlation Coefficient (ECC) [8] has also been shown to successfully align single channel images to generate multi-channel images. Finally, Fast Fourier Transform (FFT) [9] image registration methods are generally insensitive to translation, rotation, scaling, and noise, with the added benefit of being computationally efficient. Each of these methods can return a success rate and similarity score (as a measure of alignment confidence) for each registration by calculating the image similarity after image registration.

The computational cost of directly aligning gigapixel WSIs can be prohibitively high, so a smaller “image patch”-based method is often required. By virtue of their smaller size, patch-based methods do not contain as much texture information to use for registration, which can ultimately lead to poor image alignments. To address these issues, Rosetti et al. [3] proposed a method to align images at lower resolution level and propagate the registration offset to high resolutions. However, they assume that tissue contours are relatively unchanged in the grayscale space – which is not the case between H&E and IHC. Obando’s method [10] refines the common information between downsampled images before attempting registration, whereas Trahearn’s method [5] filters regions based on entropy, thresholds, and texture features.

There are several drawbacks to all these methods. First, WSIs with different stains may look quite different in hue and contrast. This can cause methods that rely on finding key points (key point matching) to fail, yielding more failures to align as too few suitable correlations in the images can be found. The other major problem is that the registration errors in low-resolution images will be magnified dozens of times if the transformation is directly applied to high-resolution levels. Therefore, a more accurate way to leverage the information from lower resolution to high resolution is needed.

In this paper, we proposed a robust strategy for WSI co-registration which can precisely and efficiently align re-stained WSIs of the same tissue sections. Our approach leverages image patches from the information-rich low resolution layers, weights their offsets by kernel density estimation (KDE), and then regresses against the hierarchical nature of WSIs to refine the offset parameters between two WSIs. Our results suggest that simple rigid image registration that incorporates the unique structure of WSI file hierarchy is well suited to address the re-stained WSI registration tasks.

Method

The main workflow of our registration strategy has been illustrated in **Fig 1**. There are multiple scaled image levels in WSIs. We extracted image patches from the top three image levels (the lowest resolution), and adopted Fourier transforms-based image registration to align H&E and IHC pairs to each level. Since there are linear relationships between image levels, we proposed a weighted hierarchical linear regression method to get the optimal registration offset and rotation angle. Generally, our approach consists of three main parts: 1) image patch-based registration; 2) KDE; 3) hierarchical resolution regression

Fig 1. **An overview of our proposed method**. The first step is get raw registration result from top three whole slide image levels. The second step is adopting Kernel Density Estimation to weight the raw registration. The last step is using hierarchical linear regression to get the optimal co-registration for whole slide images.

Image patch-based registration

In order to leverage low-level image features in WSIs, we introduced Fourier transform based image registration [11]. The goal of image registration is to determine a transformation that maximizes the similarity between two images. The image registration problem can be formulated as: $\mathrm{I}' = \mathrm{T} \cdot \mathrm{I}$, in which I denotes the original image, and I' denotes the transformed image. In our histological image registration task, there is no scale and affine transformation, because we want to align the re-stained slides under the same magnification. For a two-dimensional image registration problem, the transformation matrix T can be written like below.

$$T = \begin{bmatrix} 0 & \Delta_x \\ 0 & \Delta_y \end{bmatrix}, \quad (1)$$

where Δ_x and Δ_y denote x and y offsets, respectively. If $f_2(x, y)$ is a translated and rotated replica of $f_1(x, y)$ with translation (Δ_x, Δ_y), then

$$f_2(x, y) = f_1(x - \Delta_x, y - \Delta_y). \quad (2)$$

According to the Fourier translation and rotation properties, transforms of f_1 and f_2 are related by

$$F_2(\xi, \eta) = \mathrm{e}^{-\mathrm{j}2\pi(\xi\Delta_x + \eta\Delta_y)} \times F_1(\xi, \eta). \quad (3)$$

The cross-power spectrum of two images is defined as

$$\frac{F_1 * F_2^*}{|F_1 * F_2^*|} = e^{j2\pi(\xi\Delta_x + \eta\Delta_y)}, \quad (4)$$

where F_2^* is the complex conjugate of F_2. The shift theorem guarantees that the phase of the cross-power spectrum is equivalent to the phase difference between the images. By taking the inverse Fourier transform of the representation in the frequency domain, we have an impulse function that is approximately zero everywhere except at the displacement that is needed to optimally register the two images. We choose the "imreg_dft" library [12] as the basis of our framework, which is an implementation of discrete Fourier transformation based image registration [13].

Kernel Density Estimation

Fourier transforms-based image registration method provides a straightforward approach to align two image patches. We initially tried to directly register pathological image pairs together in highest resolution with this method, and found that most pairs of patches can be aligned well, but several failed due to limited texture information for use in defining key points. To overcome this limitation, offsets were computed from multiple patches sampled from the same WSI and at the same resolution. At first, we simply computed the mean offset in the x and y planes, but found this approach was highly variable (**Fig 2**). Instead, we introduced a KDE algorithm [14] to estimate the most possible offset for a robust image alignment.

Fig 2. **Registration offsets (mean and 1 standard deviation) including four different methods on four image levels.** The first row represents the horizontal offset; the second row represents the vertical offset. Each column represents the offset between an H&E-IHC WSI pair.

KDE is a non-parametric method to estimate the probability density function of a random variable, which can be defined as follows:

$$\hat{f}_h(x) = \frac{1}{n}\sum_{i=1}^{n} K_h(x - x_i) = \frac{1}{nh}\sum_{i=1}^{n} K(\frac{x - x_i}{h}), \tag{5}$$

where x_i is a sampled observation, n is the sample size, $\hat{f}(\cdot)$ is an estimate the probability density function of x, $K(\cdot)$ is a non-negative kernel function, and h > 0 is the bandwidth smoothing parameter. This formula can also estimate image rotation, θ. In our study, the registration offset (x, y) is a two-dimensional variable, so the KDE with a Gaussian kernel can be defined as:

$$\hat{f}_h(x, y) = \frac{1}{nh_x h_y}\sum_{i=1}^{n} K(\frac{x - X_i}{h_x}, \frac{y - Y_i}{h_y}). \tag{6}$$

We apply the Scott's rule [15] to define bandwidth, and let the bandwidth be the same on both x and y directions, such that

$$h_x = n^{\frac{-1}{(d+4)}}, \tag{7}$$

where d is the dimensionality of each data point. In our study, we let $h_x = h_y = h_{xy} = h_{yx}$ because we have no prior knowledge about the offset distribution.

Since there is no bias in the choice of image patches during image registration, we can arbitrarily use Gaussian approximation as our kernel function:

$$g(x) = \frac{1}{\sigma\sqrt{2\pi}} e^{-\frac{1}{2}\left(\frac{x-u}{\sigma}\right)^2}. \tag{8}$$

With a Gaussian kernel, the estimator is the weighted sum of the bivariate normal densities:

$$\hat{f}_h(x,y) = \frac{1}{2\pi n\sqrt{\det(HH_2)}} \sum_{i=1}^{n} \exp\left(-\frac{1}{2}(x - X_i, y - Y_i)H(x - X_i, y - Y_i)^T\right), \tag{9}$$

where (X, Y) denotes the registration offsets. The matrix H is the covariance matrix expressed in terms of bandwidth, as defined in formula (7).

We can regard the density estimates as the measures of confidence to weight the offset and angle for image pairs. Density estimation for every registration offset can be denoted as $\hat{f}(x_i, y_i)$, and normalized the confidence to [0,1]. By applying KDE, we mitigate the influence of registration errors by down-weighting their contribution to estimates of overall registration offsets and rotation angles.

Hierarchical Resolution Regression

There are several levels in a WSI (**Fig 1**), which are defined by the multi-resolution pyramidal data structure. The histological image pairs could be very different in details at lower levels (with high resolution), but appear similar in higher levels (with low resolution). This phenomenon is especially common in consecutive tissue sections. If the registration is performed only at the lowest resolution, the image registration may fail due to the weak texture information in some areas. Considering there are many image patches available at each image level, we can develop a robust method by calibrating the registration offsets across different image levels.

To find the pixel correlations across image levels, we investigated the relationship of registration offsets for two image levels. If we denote a pixel offset $\mathrm{p}(\mathrm{x},\mathrm{y})$ in level 1 with image resolution R_1, and denote the corresponding pixel offset $\mathrm{p}(\mathrm{x}',\mathrm{y}')$ in level 2 with image resolution R_2, and the downsampling factor between image levels is known and fixed, it follows that pixel correlations can be defined as:

$$p(x,y) = \frac{R1}{R2} p(x',y'), \tag{10}$$

So, if we apply image registration on two different image levels, in ideal conditions, the linear regression of offsets should be a line that goes through the origin. A weighted linear regression strategy can be used to adaptively learn the exact linear relationship. Therefore, the cost function of the regression problem can be interpreted as:

$$c(m) = \frac{1}{N}\sum_{l=1}^{L}\sum_{i=0}^{N} R_l * \widehat{f}_l\left(x_i^l, y_i^l\right) * \left(y_i^l - m x_i^l\right) \tag{11}$$

where $R_l \in \{0.25, 0.25, 0.5\}$ denotes the resolution ratio of current image level to lower image level, $L \in [1,3]$ denotes the image levels, N represents the number of image patches used at each level, and $\hat{f}(x_i, y_i)$ is calculated from formula (9). By minimizing this cost function, the optimal slope m for cross-level image registration can be determined.

Experimental Data

Data Description

We collected three pairs of WSIs for our experiments. They are serial sections from a specimen of breast cancer. Each pair consists of an H&E and an IHC image of the same

tissue section, including Caspase 3, KI67 and PHH3, respectively. OpenSlide [16], a public C library was introduced to extract image patches from a specific coordinate and image level. There are four image levels in each WSI: levels 0-3, where level 0 denotes the original image with highest resolution and level 3 denotes the down-sampled image with lowest resolution. The resolution ratio of image levels for our dataset is 1:4:16:32 (from level 3 to level 0), with a pixel size is 0.25μm at the highest resolution.

Ground Truth Annotation

There is no general quantified evaluation metric for image registration of multiple WSIs. To evaluate the registration accuracy, we developed an image visualization tool to manually align two WSI by adjusting a floating image's offset and rotation angle with respect to a fixed image (**Fig 3**). The ground truth of image registration for our dataset was determined by comparing the details at the same position after careful manual adjustment of the floating image. We have made this tool freely available for others to use in their own projects. [1]https://github.com/smujiang/Re-stained_WSIs_Registration

Figure 3. Screen shot of WSI registration tool. After loading WSIs, the image on the right can be shifted and rotated by adjusting the x and y offset positions. A green cross is attached to mouse cursor, so that details of two images at the same location can be compared easily. Source code of this tool can be found at our GitHub[1].

Experiments and Results

Our experiments were conducted as illustrated in the workflow (**Fig 1**), which consists of three main steps: 1) raw registration, 2) KDE weighting, and 3) hierarchical linear regression.

Raw Registration

We co-registered 100 pairs of H&E-IHC patches on all WSI levels using three rigid registration methods: ECC [8], FFT [9], and SIFT [7]. To improve registration accuracy, we also tried to add an extra filter to distill the matched key points detected by RANSAC [17] in traditional SIFT output, which is denoted as SIFT-ENH. T he extra filter keeps key points that share a similar slope. All implementations of these methods are based on the OpenCV API [18]. We applied FFT together with these three methods to our dataset, the statistical features of registration results are shown in **Fig 2**. The ECC, FFT, SIFT and SIFT_ENH all performs well on lower resolutions (levels 2-3), but poor at level 0.

KDE Weighting

To reduce the variance in the predicted offsets, we attempted two different types of procedures: weighting based on raw registration score and KDE. All the image registration methods assessed here return a score to measure the success of registration. However, we found that these scores do not always reflect the registration success for many patch-level registrations. The reason might come from the fact that H&E and IHC images are very different in hue and texture, and some have sparse unique local details. To reveal this phenomenon, we show an example (**Fig4**, top row) by drawing the registration offsets in two dimensional coordinates, where each registration is represented as a dot, colored by confidence score. High scores mean the registration algorithm has high confidence in its offset estimation. We found that offsets close to the ground truth are not necessarily those

with higher scores. This deficiency implies that confidence score based on image similarity cannot effectively measure the registration accuracy, and a more efficient way should be adopted. Hence, we show the KDE algorithm is more accurate at predicting the higher scoring alignments than native scoring methods (**Fig 4**, bottom row).

Figure 4. Comparison of KDE and similarity score on reflecting registration success. Scatterplots of co-registration offsets at different image levels. Top row: colored with similarity score; Bottom row: colored with KDE. In each subplot, a dot with cold color means registrations with low confidence level, while a dot with hot color means registrations with high confidence level.

Hierarchical Resolution Regression

As shown in **Fig 2**, the error in offset prediction is strongly correlated with level being viewed. Since image offsets across WSI levels obey a linear downsampling strategy to build their intrinsic pyramidal structure, we introduced linear regression to extrapolate the level 0 offsets. **Fig 5**, we draw the registration results of each image level as scatters, and also draw the line to show their weighted linear regressions. For the each WSI pair, the FFT-based regression performed well, with the regression based on either the raw image registration scores was not different from the KDE-weighting scheme. However, the same WSI pair using an alternative raw image registration method (SIFT) was more varied and showed substantial improvement when using the KDE weights rather than the scoring weights.

Figure 5. **Hierarchical linear regression result of registration.** Registration results of each image level were displayed into dots with different shapes. Weighted with similarity

score and KDE confidence value, linear regression results are shown in straight lines with different colors. Ground truth is shown in a blue cross.

The FFT based method can routinely performs well on our dataset, and there is no apparent difference when differentially weighting the offsets. However, this is not consistent among methods. In particular, the ECC method can result in dramatically different multilevel regressions when weighting using the similarity scoring metric rather than our KDE approach. A comparison of our approach versus the similarity score based offsets is shown for each slide, axis, and method in **Fig 6**.

Figure 6. **Final regression-based offset calculation using scoring and the KDE-based method.** Each slide was tested with each raw image registration method and regressed to find the true offset. The numbers here represent the difference between the true (manually curated) offset and the extrapolated offset. The SIFT_ENH model is an attempt to select the best key points from SIFT to improve accuracy. It clearly shows the benefit of using the KDE-based regression, as most of the error is at or near 0.

Discussion

In this paper, we proposed an approach that combines traditional rigid image registration methods into a framework that leverages the hierarchical nature of WSIs. We showed the strong advantages of incorporating KDE to better estimate the true offsets compared to the similarity score based approaches. By comparing multiple image registration methods, including FFT, ECC SIFT, and SIFT-ENH, we found that the FFT-based method outperformed than others for our image registration tasks. However, we were able to further increase the precision of the FFT registration by incorporating our KDE-weighted linear regression.

The main limitation of our research is that our method has only been tested on three WSIs of different stains, and not serial sections. Consecutive sections are not identical in their cellular structure and composition, thus requiring non-rigid image registration techniques. However, we posit that KDE will still provide a more reliable estimate in this scenario. Furthermore, as our method can be used to match large numbers of image pairs with reliable alignment scores, it provides a scalable framework to collect samples to train a deep neural network, where deep textural patterns beneficial for image alignment can be learned.

The most distinctive part of our work is that we introduced KDE to distill the raw registration result. As most registration methods may return a confidence value for each registration, improper trust in such scores can lead to poor quality results. We show that similarity of the two images after transformation does not always reflect whether the registration was a success or not. Moreover, these approaches do not fully utilize all available data to ensure maximal accuracy. For example, it is common for many small image patches to be analyzed for a given slide in digital pathology. Each of these patches should have nearly identical x and y offsets. Also, the x and y offsets should follow a fixed linear trend between high and low magnification. By combining the x and y offset estimates across multiple patches from the same slide with the different z magnifications, we have proposed a more robust way to estimate a true x and y offset for each magnification level.

Acknowledgements

This study is supported by the Division of Laboratory Medicine and Pathology (TJF, SNH) and the Leon Lowenstein Foundation (SNH).

References

1. Lotz, J., et al. *Zooming in: high resolution 3D reconstruction of differently stained histological whole slide images*. in *Medical Imaging 2014: Digital Pathology*. 2014. San Diego, California: SPIE.
2. Lotz, J., et al., *Patch-Based Nonlinear Image Registration for Gigapixel Whole Slide Images.* IEEE Trans Biomed Eng, 2016. **63**(9): p. 1812-1819.
3. Rossetti, B.J., et al., *Dynamic Registration for Gigapixel Serial Whole Slide Images.* Proc IEEE Int Symp Biomed Imaging, 2017. **2017**: p. 424-428.
4. Solorzano, L., et al., *Whole Slide Image Registration for the Study of Tumor Heterogeneity*, in *Computational Pathology and Ophthalmic Medical Image Analysis*, T.Z. Stoyanov D, Ciomp F, Xu Y, Martel A, Maier-Hein L, Rajpoot N, van der Laak J, Veta M, McKenna S, Snead D, Trucco E, Garvin MK, Chen XJ, Bogunovic H, Editor. 2018, Springer International Publishing: Switzerland. p. 95-102.
5. Trahearn, N., et al., *Hyper-Stain Inspector: A Framework for Robust Registration and Localised Co-Expression Analysis of Multiple Whole-Slide Images of Serial Histology Sections.* Scientific Reports, 2017. **7**(1): p. 5641.
6. Mueller, D., D. Vossen, and B. Hulsken, *Real-time deformable registration of multi-modal whole slides for digital pathology.* Comput Med Imaging Graph, 2011. **35**(7-8): p. 542-56.
7. Lowe, D., *Distrinctive Image Features from Scale-Invariant Keypoints.* International Journal of Computer Vision, 2004. **60**(2): p. 91-110.
8. Evangelidis, G.D. and E.Z. Psarakis, *Parametric image alignment using enhanced correlation coefficient maximization.* IEEE Trans Pattern Anal Mach Intell, 2008. **30**(10): p. 1858-65.

9. Atta-Fosu, T. and W. Guo, *Joint Segmentation and Nonlinear Registration Using Fast Fourier Transform and Total Variation - WiSH2, Sirince, Turkey, June 2016*, in *Research in Shape Analysis*, L.K. Genctav A, Tari S, Hubert E, Morin G, El-Zehiry N, Chambers E, Editor. 2018, Springer International Publishing: Switzerland. p. 111-132.

10. Obando, D., et al. *Multi-Staining Registration of Large Histology Images*. in *2017 IEEE 14TH International Symposium on Biomedical Imaging*. 2017. Melbourne, Australia.

11. Reddy, B.S. and B.N. Chatterji, *An FFT-based technique for translation, rotation, and scale-invariant image registration.* IEEE Trans Image Process, 1996. **5**(8): p. 1266-71.

12. Tyc, M. and C. Gohlke. *Welcome to imreg_dft's documentation*. Read the Docs 2014; Available from: https://imreg-dft.readthedocs.io/en/latest/.

13. Matungka, R., Y.F. Zheng, and R.L. Ewing, *Image registration using adaptive polar transform.* IEEE Trans Image Process, 2009. **18**(10): p. 2340-54.

14. Chen, Y.-C., *A tutorial on kernel density estimation and recent advances.* Biostatistics & Epidemiology, 2017. **1**(1): p. 161-187.

15. Heidenreich, N., A. Schindler, and S. Sperlich, *Bandwidth selection for kernel density estimation: a review of fully automatic selectors.* AStA Advances in Statistical Analysis, 2013. **97**(4): p. 403-433.

16. Goode, A., et al., *OpenSlide: A vendor-neutral software foundation for digital pathology.* J Pathol Inform, 2013. **4**: p. 27.

17. Fischler, M. and R. Bolles, *Random sample consensus: a paradigm for model fitting with applications to image analysis and automated cartography*. Communications of the ACM, 1981. **24**(6): p. 381-395.

18. Culjak, I., et al. *A brief introduction to OpenCV*. in *35th International Convention MIPRO*. 2012. Opatija, Croatia: IEEE.

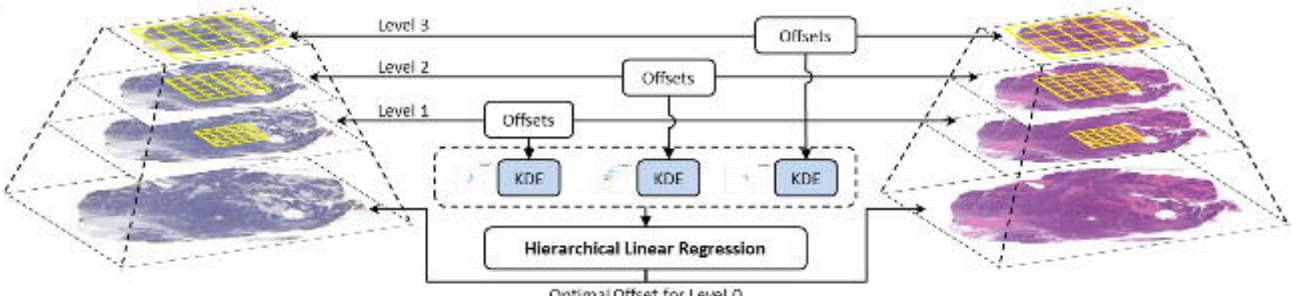
Level 3
Offsets
Level 2
Offsets
Level 1
Offsets
KDE
KDE
KDE
Hierarchical Linear Regression
Optimal Offset for Level 0

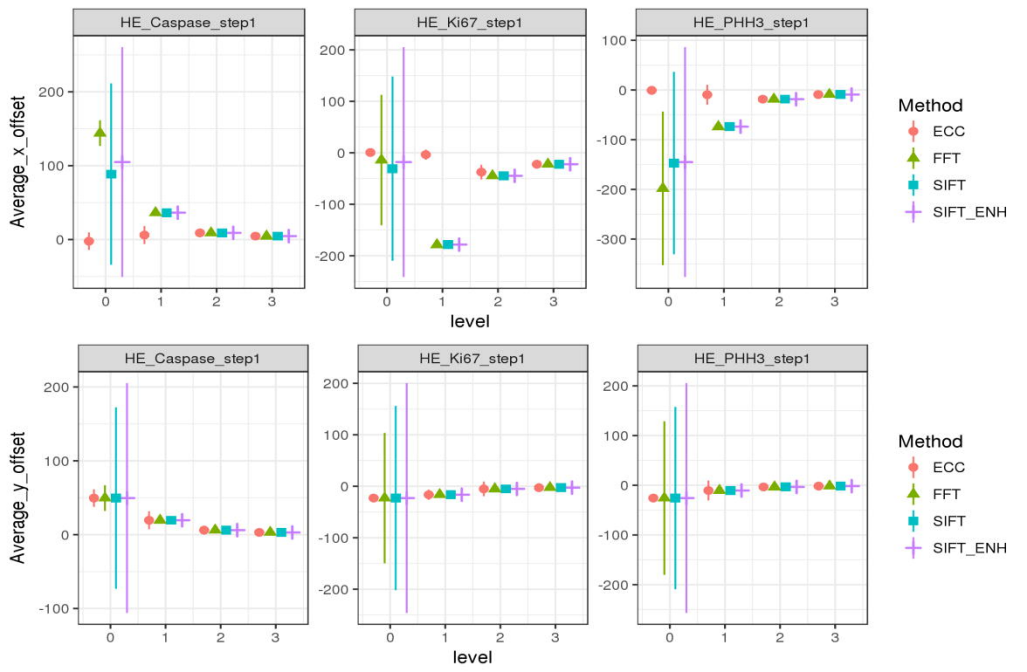
HE_Caspase_step1
HE_Ki67_step1
HE_PHH3_step1
Average_x_offset
Average_y_offset
level
Method
ECC
FFT
SIFT
SIFT_ENH

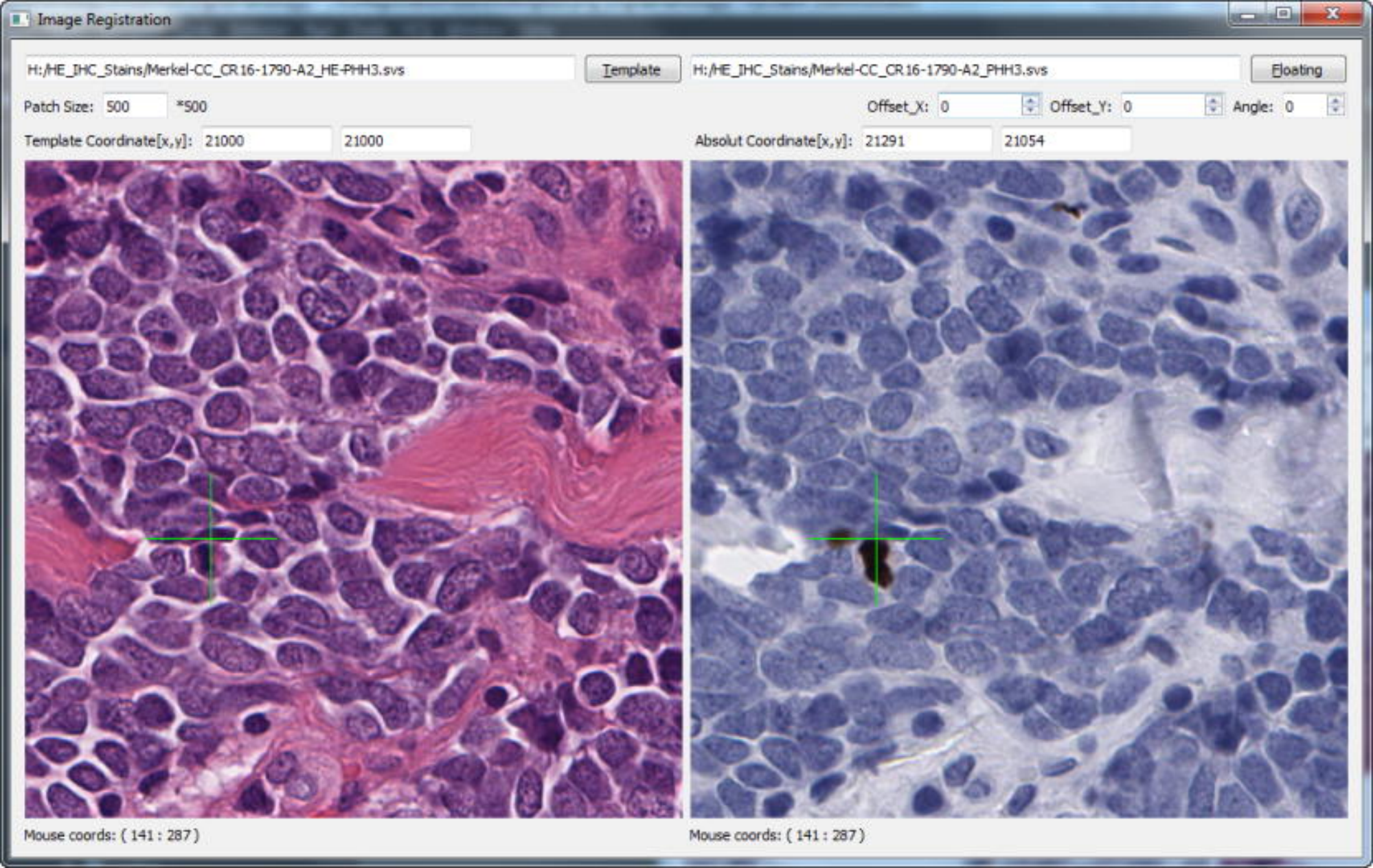
Image Registration
H:/HE_IHC_Stains/Merkel-CC_CR16-1790-A2_HE-PHH3.svs
Template
H:/HE_IHC_Stains/Merkel-CC_CR16-1790-A2_PHH3.svs
Floating
Patch Size: 500 *500
Offset_X: 0
Offset_Y: 0
Angle: 0
Template Coordinate[x,y]: 21000 21000
Absolut Coordinate[x,y]: 21291 21054
Mouse coords: (141 : 287)
Mouse coords: (141 : 287)

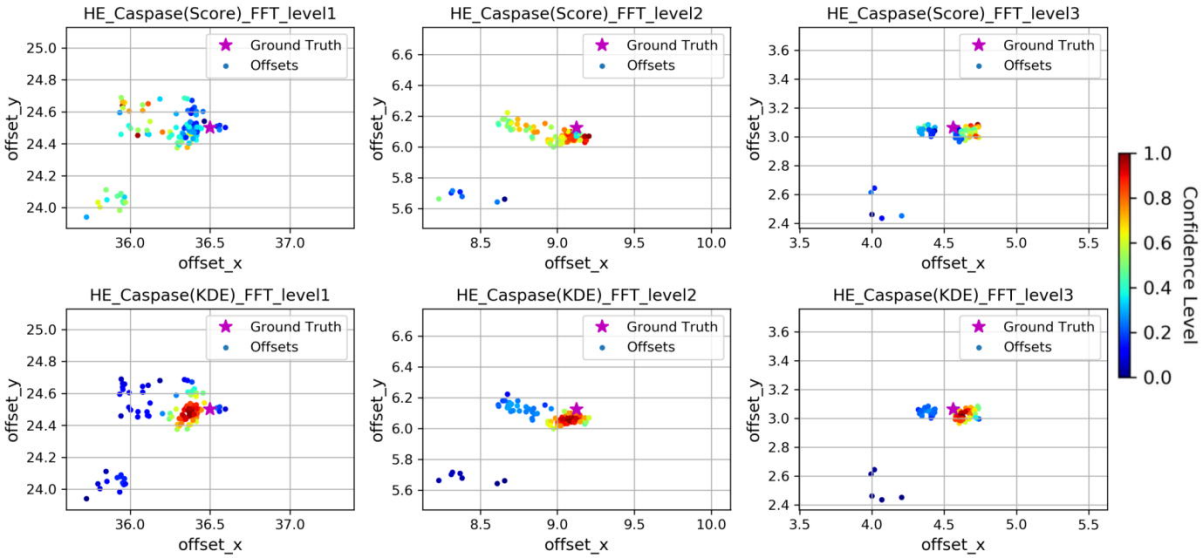
HE_Caspase(Score)_FFT_level1
HE_Caspase(Score)_FFT_level2
HE_Caspase(Score)_FFT_level3
HE_Caspase(KDE)_FFT_level1
HE_Caspase(KDE)_FFT_level2
HE_Caspase(KDE)_FFT_level3
Ground Truth
Offsets
offset_x
offset_y
Confidence Level

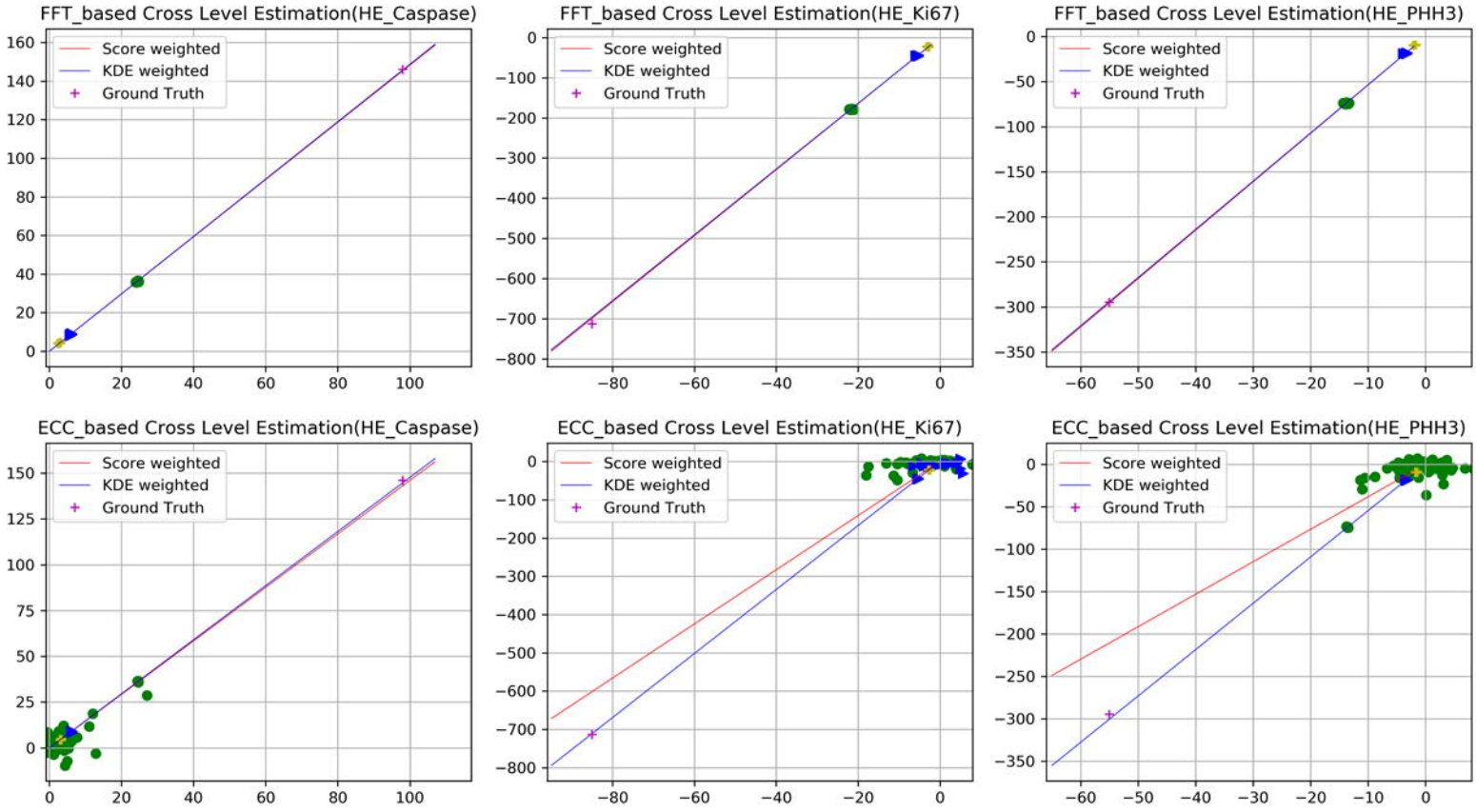
FFT_based Cross Level Estimation(HE_Caspase)
FFT_based Cross Level Estimation(HE_Ki67)
FFT_based Cross Level Estimation(HE_PHH3)
ECC_based Cross Level Estimation(HE_Caspase)
ECC_based Cross Level Estimation(HE_Ki67)
ECC_based Cross Level Estimation(HE_PHH3)
Score weighted
KDE weighted
Ground Truth

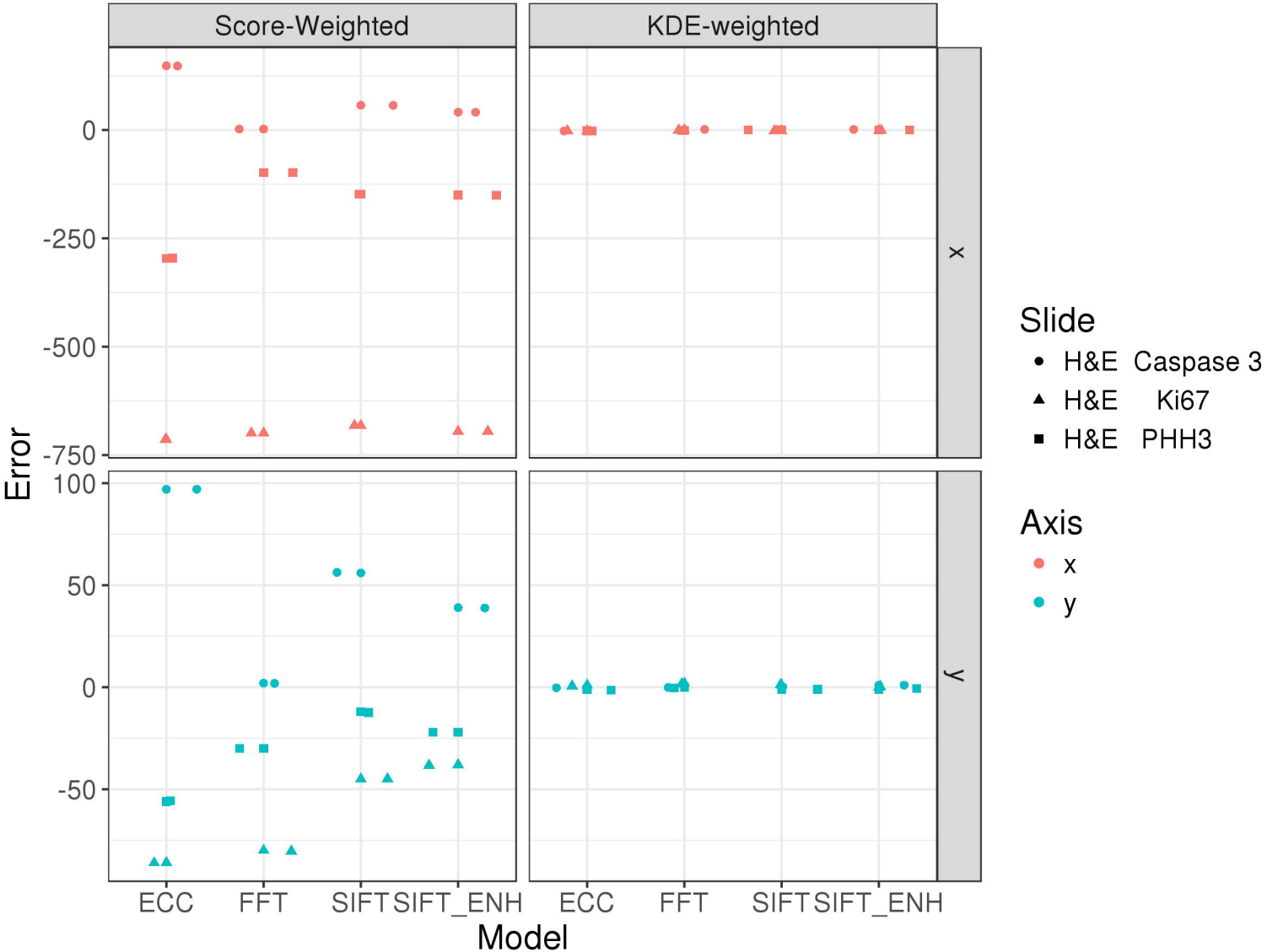
Score-Weighted
KDE-weighted
x
y
Error
0
-250
-500
-750
100
50
0
-50
ECC
FFT
SIFT
SIFT_ENH
Model
Slide
H&E Caspase 3
H&E Ki67
H&E PHH3
Axis
x
y